GALAXY DISKS DO NOT NEED TO SURVIVE IN THE Λ -CDM PARADIGM: THE GALAXY MERGER RATE OUT TO Z \sim 1.5 FROM MORPHO-KINEMATIC DATA.

 $\begin{array}{l} \text{M. Puech}^1, \text{ F. Hammer}^1, \text{ P.F. Hopkins}^2, \text{ E. Athanassoula}^3, \text{ H. Flores}^1, \text{ M. Rodrigues}^{4,1,5}, \text{ J.L. Wang}^1, \text{ and Y.B.} \\ & \text{Yang}^{1,6} \end{array}$

¹GEPI, Observatoire de Paris, CNRS-UMR8111, Univ. Paris-Diderot, 5 place Janssen, 92195 Meudon, France
 ²Department of Astronomy, University of California, Berkeley, CA 94720, USA
 ³Laboratoire d'Astrophysique de Marseille, Observatoire Astronomique de Marseille Provence, Technopole de l'toile - Site de Chateau-Gombert, 38 rue Frdric Joliot-Curie, 13388 Marseille Cedex 13, France
 ⁴European Southern Observatory, Alonso de Cordova 3107 - Casilla 19001 - Vitacura -Santiago, Chile
 ⁵CENTRA, Instituto Superior Tecnico, Av. Rovisco Pais 1049-001 Lisboa, Portugal and
 ⁶National Astronomical Observatories, Chinese Academy of Sciences, 20A Datun Road, Chaoyang District, Beijing 100012, China
 Submitted to ApJ

ABSTRACT

About two-thirds of present-day, large galaxies are spirals such as the Milky Way or Andromeda, but the way their thin rotating disks formed remains uncertain. Observations have revealed that half of their progenitors, six billion years ago, had peculiar morphologies and/or kinematics, which exclude them from the Hubble sequence. Major mergers, i.e., fusions between galaxies of similar mass, are found to be the likeliest driver for such strong peculiarities. However, thin disks are fragile and easily destroyed by such violent collisions, which creates a critical tension between the observed fraction of thin disks and their survival within the Λ -CDM paradigm. Here we show that the observed high occurrence of mergers amongst their progenitors is only apparent and is resolved when using morphokinematic observations which are sensitive to all the phases of the merging process. This provides an original way of narrowing down observational estimates of the galaxy merger rate and leads to a perfect match with predictions by state-of-the-art Λ-CDM semi-empirical models with no particular fine-tuning needed. These results imply that half of local thin disks do not survive but are actually rebuilt after a gas-rich major merger occurring in the past nine billion years, i.e., two-thirds of the lifetime of the Universe. This emphasizes the need to study how thin disks can form in halos with a more active merger history than previously considered, and to investigate what is the origin of the gas reservoir from which local disks would reform.

Subject headings: galaxies: evolution, galaxies: formation, galaxies: interactions, galaxies: kinematics and dynamics, galaxies: general

1. INTRODUCTION

Over the past years, observations and theory have been progressing significantly in understanding how the first large disk galaxies could form. Near-infrared (rest-frame optical) imaging from the HST reveals that, while $\sim 40\%$ of z~1-3 most massive (i.e., $M_{stellar} \geq 5 \times 10^{10} M_{\odot}$) galaxies are relatively compact and quiescent, ~60% of them are actively forming stars and show quite extended stellar structures (Weinzirl et al. 2011; see also van Dokkum et al. 2011; Förster Schreiber et al. 2011). In a larger range of mass (i.e., $\sim 10^9$ - $10^{11} M_{\odot}$), Law et al. (2012) suggested that the stellar phase of $z\sim1.5-3.6$ galaxies is probably distributed as triaxial ellipsoids rather than thick disks. Integral field spectroscopy now routinely provides us with spatially-resolved kinematics of the sub-population of z~1-3 emission line galax-(Förster Schreiber et al. 2006; ies Bournaud et al. 2008; van Starkenburg et al. 2008: Wright et al. 2009; Förster-Schreiber et al. 2009; Law et al. 2009; Epinat et al. 2009; Lemoine-Busserolle et al. 2010; Lemoine-Busserolle & Lamareille 2010; Contini et al. 2012; Epinat et al. 2012). Actively forming galaxies at these epochs reveal a relatively balanced mix of obvious (major) mergers, relatively compact dispersionsupported objects, and rotating extended structures, all being much more turbulent in their gaseous phase

compared to local galaxies (Förster-Schreiber et al. 2009). On the theoretical side, cosmological simulations have predicted that streams of cold gas would occur in the halos in which these galaxies are expected to inhabit (Dekel et al. 2009; Keres et al. 2009; Agertz et al. 2009; Brooks et al. 2009; Ceverino et al. 2010; van de Voort et al. 2011). Such streams would be responsible for bringing a continuous amount of high angular momentum gas in these halos over a relatively short timescale (Kimm et al. 2011; Pichon et al. Because the amount of mass brought that way is expected to be considerable, this could in principle pressurize the central forming disk and result in clump fragmentation (Dekel et al. 2009b; Bournaud et al. 2009; Genzel et al. 2011), as ubiquitously observed at these epochs (Elmegreen et al. 2005, 2009,b). Such "clumpy galaxies" are now more and more considered as an important step of galaxy formation. However, it remains unclear whether the lifetime of such clumps is long enough to allow them to survive feedback effects and coalesce to form a central bulge (Elmegreen et al. 2008; Bournaud et al. 2009b; Murray et al. 2010; Krumholz & Dekel 2010; 2010; Genel et al. Förster Schreiber et al. Powell et al. 2011; Hopkins et al. 2011). It remains also unclear how thin disks can form from the high angular momentum gas which is expected to be accreted into

the halos. Finally, the smoking gun detection of cold gas accretion is still missing, although different options are being extensively discussed (Dijkstra & Loeb 2009; Steidel et al. 2010; Goerdt et al. 2010; Benson & Bower 2011; Faucher-Giguère & Kereš 2011; Fumagalli et al. 2011; Kimm et al. 2011b; Le Tiran et al. 2011; Giavalisco et al. 2011; Stewart et al. 2011,b).

In contrast, it remains more uncertain how these $z\sim2$ thick rotating disks evolved down to $z\sim0$, and how the local thin disks formed. Indeed, the Hubble sequence of galaxies such as the Milky Way $(M_{stellar} = 10^{10-11} M_{\odot})$ reveals a predominance (72%) of rotationally-supported disks in the present-day Universe (Delgado-Serrano et al. 2010). Using the Cosmological Principle, their progenitors at z~0.6, i.e., six billion years ago, can be selected and their morphology studied using the Advanced Camera for Survey on-board the Hubble Space Telescope (Delgado-Serrano et al. 2010). Using methodologies and rest-frame luminosities that mimic those used for local galaxies, the likeliest ancestor of the Hubble sequence can then be established (Delgado-Serrano et al. 2010). Half the progenitors of spiral galaxies show peculiar morphologies that exclude them from this sequence (van den Bergh 2002; Delgado-Serrano et al. Most of them are starbursts, whose emer-2010). gence at $z\sim0.6$ reflects that of emission line galaxies (Hammer et al. 1997; Mignoli et al. 2005). As part of the IMAGES survey, the large-scale spatially-resolved kinematics of a representative subsample of 63 emission line galaxies at z=[0.4-0.75] was obtained using the GIRAFFE multi-IFU spectrograph (Flores et al. 2006; Puech et al. 2006; Yang et al. 2008). Most peculiar galaxies also reveal peculiar large-scale motions (Neichel et al. 2008). Comparing the morpho-kinematic properties of the subsample of the 33 galaxies lying into the CDFS (Yang et al. 2008) with those of a grid of simple major merger models, convincing matches were found in about two-thirds of the cases (Hammer et al. 2009). This leads to at least one third of the progenitors of present-day spirals potentially involved in a major merger. Since major mergers can easily destroy thin rotating disks (Toomre & Toomre 1972; Toomre 1977; Barnes 1988, 1992; Hernquist 1993; Barnes& Hernquist 1996; Toth & Ostriker 1992; Hopkins et al. 2008), this creates a critical tension between the large fraction of present-day disks and their survival within the Λ -CDM paradigm (Stewart et al. 2008; Weinzirl et al. 2009).

Further investigating the "disk survival issue" requires an accurate estimation of the evolution of the merger rate, i.e., the fraction of galaxy involved in mergers per unit time. Several techniques were developed over the past years to try to quantify accurately the evolution of the merger rate, such as the pair technique (e.g., Le Févre et al. 2000; Kartaltepe et al. 2007; Lin et al. 2008; Rawat et al. 2008; Ryan et al. 2008; Bundy et al. 2009; de Ravel et al. 2009, 2011) or the morphological technique, either through non-parametric (e.g., Conselice et al. 2003; Lotz et al. 2008; Conselice et al. 2009; Shi et al. 2009; López-Sanjuan et al. 2009) or visual (e.g., Jogee et al. 2009; Bridge et al. 2010) classifications. Alternatively, the amplitude of the twopoint correlation function can also be used to infer a merger rate (Bell et al. 2006; Robaina et al. 2010). All these techniques are very dependent on the visibility

timescale of the specific merging phase sampled by the observations, which requires to be estimated using additional numerical simulations and/or analytical arguments (Lotz et al. 2008b). Accounting for the exact distributions of merger mass ratios or orbits involved is also challenging (Lotz et al. 2010,b, 2011). As a result, observational estimates spread over almost one decade at $z\sim0-1$ (Hopkins et al. 2009; Lotz et al. 2011).

Recent progresses combine numerical simulations with transfer radiation to derive a weighted average visibility timescale for each observational technique, using predictions for the distribution of mass ratios and other merger parameters from galaxy formation models (Lotz et al. 2011). Taking these aspects into account, the discrepancy between the different merger rates derived in the literature is significantly reduced, while remaining differences are attributed to differences in range of mass ratio and sample selection (Lotz et al. 2011). This illustrates how crucial it is to carefully accounts for these aforementioned effects. The present study puts this effort one step forward: we show that by combining spatially-resolved morphological and kinematic data as those provided by the IMAGES survey, one can date back the epoch where observed galaxy mergers were still in pair, and then derive the evolution of the fraction of mergers out to $z\sim1.5$. in a consistent way as a function of redshift. Such data also allow us to estimate relevant visibility timescales that are by construction consistent with the distribution of merger mass ratios and orbits of the galaxies in the observed sample. The derived evolution of the merger rate out to $z\sim1.5$ is found to be within a factor 2-3 of theoretical predictions from a state-of-the-art Λ -CDM semiempirical model.

This paper is organized as follows. Sect. 2 presents the data used in this paper, which come from the IMAGES survey of $z\sim0.6$ emission line intermediate-mass galaxies. In Sect. 3, we argue why large morpho-kinematic perturbances most likely result from major mergers. Sect. 4 presents the major merger fractions and rates derived from these data. A comparison with state-of-the-art semi-empirical model of galaxy formation is presented in Sect. 5. Finally, a discussion is given in Sect. 6 and conclusions are drawn in Sect. 7. Throughout the paper, magnitudes are given in the AB system, and a WMAP-7 cosmology is used (Komatsu et al. 2011), with $(\Omega_m,$ Ω_{Λ} , Ω_b , h, σ_8)=(0.275, 0.725, 0.0458, 0.702, 0.816). We adopt the diet Salpeter IMF (Bell et al. 2003) throughout this paper. Note that all IMF-dependant quantities cited from other studies were converted to this IMF.

2. MORPHO-KINEMATIC DATA OF Z=[0.4, 0.75] GALAXIES: SUMMARY OF THE IMAGES SURVEY

2.1. The representative IMAGES-CDFS sample

In the frame of the IMAGES survey, a sample of 35 emission line galaxies at z=[0.4-0.75], i.e., about six billion years ago (mean/median redshift of z=0.6/0.65), were observed in the Chandra Deep Field South (CDFS) (Yang et al. 2008). This subsample of IMAGES is of particular interest since it benefits from homogeneous imaging and 3D data (Yang et al. 2008; Neichel et al. 2008). IMAGES targets were selected to have $I_{AB} \leq 23.5$ and $EW_0([OII]) \geq 15 \text{Å}$ to guarantee their detection by the multi-IFU spectrograph FLAMES/GIRAFFE at VLT (Ravikumar et al. 2007; Flores et al. 2006). These

galaxies were selected to be intermediate-mass galaxies $(M_{stellar} = 10^{10} - 10^{11} M_{\odot})$ using a diet Salpeter IMF and simplified prescriptions to convert J-band luminosity and B-V colors into stellar mass, following Bell et al. 2003). This range of mass is of particular interest since most of the star formation at z \leq 1 occurred in such galaxies (Hammer et al. 2005; Bell et al. 2005; Zheng et al. 2007). Since the fraction of E/S0 did not raise between z \sim 0.6 and z=0 (Delgado-Serrano et al. 2010), z \leq 1 intermediate-mass galaxies are the likeliest progenitors of local spirals (see also App. B).

From the full IMAGES sample, one galaxy was rejected because it turned out not to be a starburst galaxy (Hammer et al. 2009; Yang et al. 2009), and another one because the HST/ACS images were corrupted and no morphological analysis could be conducted. The resulting sample is fully representative of the J-band luminosity function at z=0.5-1.0 (Yang et al. 2008). At these redshifts, the near-infrared luminosity functions of the global population and of the blue sub-population of galaxies are very similar (Cirasuolo et al. 2007). At first order, emission-line and blue galaxies sample the same population (Delgado-Serrano et al. 2010), which in principle guarantees that the IMAGES-CDFS sample is representative of the star forming population of galaxies at these epochs.

The total SFR of all the 33 remaining galaxies in the IMAGES-CDFS sample was estimated as the sum of the unobscured SFR measured from the rest-frame UV luminosity at 2800Å combined to the dust-reprocessed contribution, which was estimated from the IR luminosity as measured using 24 μ m Spitzer fluxes (see Puech et al. 2010 for details). We find a mean SFR of $\sim 12 M_{\odot}/\text{yr}$, which compares well with other UV+IR measurements in larger samples at a similar range of mass and redshift (e.g., Jogee et al. 2009). In Fig. 1, the location of the IMAGES-CDFS galaxies in the SFR-M_{stellar} plan is compared to the sequence of starbursting galaxies observed by Noeske et al. (2007) at z=0.45-0.7. As expected, the IMAGES-CDFS sample comprises Luminous InfraRed Galaxies, which populates the high-SFR tail of the distribution at SFR≥14M_☉/yr (Le Floc'h et al. 2005), and less obscured (UV) starbursts, which populate the low-SFR tail of the distribution. This figure reveals that most (91%) IMAGES-CDFS galaxies lie well within the observed SFR- $M_{stellar}$ sequence at these redshifts. The star formation rate density in the IMAGES-CDFS sample is found to be $\log{(\rho_{sfr})} \sim 1.4$ (where ρ_{sfr} is expressed in $M_{\odot}.yr^{-1}.Mpc^{-3}$), also in good agreement with expectations from larger surveys that include IR data at 24 μm (Zheng et al. 2007).¹ This confirms that the IMAGES-CDFS sample is representative of starforming galaxies at $z\sim0.6$.

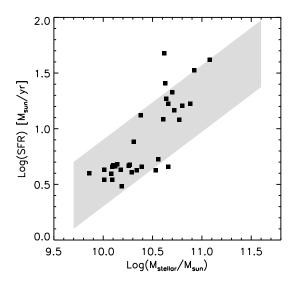


Figure 1. The SFR-Stellar mass sequence in the IMAGES-CDFS sample (black squares). SFRs and stellar masses were rescaled to a diet Salpeter IMF. The grey region represents the z=0.45-0.7 SFR-Stellar mass sequence and its ± 1 - σ scatter from Noeske et al. (2007), as reported by Dutton et al. (2010).

Gas masses were estimated from the total SFR by inverting the Schmidt-Kennicutt law (Puech et al. 2010). All galaxies were found in a range of total baryonic mass $\log{(M_b/M_\odot)}=10.2$ to 11, or $\log{(M_{stellar}/M_\odot)}$ in the range 10 to 11. The stellar-mass density in the IMAGES-CDFS sample is found to be $\log{(\rho_{stellar})} \sim 8.1$ (where $\rho_{stellar}$ is expressed in $M_\odot.Mpc^{-3}$), which is in relatively good agreement with expectations from larger surveys of blue galaxies (Arnouts et al. 2007; Bell et al. 2007), within expected uncertainties.

2.2. Morpho-kinematic classification

Detailed color morphology (at a ~ 500 pc resolution scale) and large-scale kinematics (at a ~ 7 kpc resolution scale) were obtained thanks to the Hubble Space Telescope, and 3D spectroscopy using the GIRAFFE multi-IFU spectrograph, respectively. Galaxies were classified independently according to their morphology (Neichel et al. 2008) and kinematics (Yang et al. 2008), based on similarities with the properties of local galaxies.

The kinematical maps allowed us to classify the IMAGES-CDFS galaxies into three distinct kinematic classes (see Yang et al. 2008). Rotating disks [RDs] were those for which the Velocity Field [VF] showed an order gradient, a dynamical axis aligned with the morphological axis, and a velocity dispersion peak located at the dynamical center. For these objects, it was required that the sigma peak location and amplitude can be reproduced by modeling the velocity dispersion map from the velocity gradient observed in the VF. At the GIRAFFE spatial resolution, it is indeed expected that most of the rotation curve gradient falls into on GIRAFFE pixel, which results in an velocity dispersion peak at the dynamical center of the object. Conversely, galaxies with complex kinematics [CKs] were those for which no ordered gradient was observed in the VF, or when a significant misalignment between the kinematical rotation

 $^{^1}$ Apparent discrepancies of up to a factor two can appear in comparison with other studies based on different survey areas, stellar mass cuts, and methods for estimating the SFR. For instance, Jogee et al. (2009) found $\log{(\rho_{sfr})}$ =-1.4 at z~0.6 for galaxies with $\rm M_{stellar} \geq 10^{9.1} \rm M_{\odot}$ and $\log{(\rho_{sfr})}$ =-1.9 for galaxies with $\rm M_{stellar} \geq 10^{10.5} \rm M_{\odot}$ (using a diet Salpeter IMF). Using a larger area survey, Zheng et al. (2007) found that for the mass range $\rm M_{stellar} = 10^{10.15} - 10^{11.15} \rm M_{\odot}$, i.e., very close to the range of mass considered in the present study, $\log{(\rho_{sfr})}$ ranges from -1.56 $^{+0.07}_{-0.08}$ at z=0.4-0.6 to -1.34±0.05 at z=0.5-0.8, which is consistent with the value found in the IMAGES-CDFS sample.

axis and the morphological principle axis was detected. Perturbed rotators [PRs] gathered objects with an order velocity gradient in the VF, but for which the velocity dispersion peak (location and/or amplitude) could not be reproduced from the VF, which indicates that this peak cannot be attributed to rotation. This classification was tested against quantified criteria and considering all uncertainties associated to kinematic measurements, which makes it objective and reproducible, as described extensively in Yang et al. (2008).

The detailed color morphology of all the 33 galaxies in the IMAGES-CDFS sample was studied by Neichel et al. (2008). Using a reproducible decision tree relying on parametric parameters and visual inspection of images and color maps, galaxy morphologies were classified into six different classes: Compact systems, Mergers, Peculiar/ Possible Mergers, Peculiar Tadpoles, Peculiar Irregulars, and Spiral disks. In particular, it was required for a rotating disks to show redder colors towards the center as observed in local galaxies. This classification was done by three independent classifiers using a decision tree, which limits the subjectivity and makes it reproducible. The comparison between the morphological and kinematical classes show a very good agreement, with more than 80% of spiral disks having rotating disks, and more than 90% of peculiar galaxies having complex or perturbed kinematics.

Since perturbations in the (ionized) gaseous phase generally correspond to perturbations in the stellar phase, the result of both the morphological and kinematical classifications can be robustly synthesized into a morphokinematic classification (Hammer et al. 2009). With this classification, rotating spiral disks are those classified both as rotating disks from the kinematic point of view, and as spiral disks from the morphological point of view. Non-relaxed systems are those that show a complex kinematics and a peculiar morphology. Semi-relaxed systems are galaxies that show either some rotation from their kinematics (being classified as either a rotating disk or either a perturbed rotation) but with a peculiar morphology, or galaxies that do not show rotation in their kinematics (being classified as having a complex kinematics) but with a spiral disk morphology. According to this classification, 80% of z~0.6 starburst galaxies are non-relaxed or semi-relaxed systems (Hammer et al. 2009), which corresponds to $\sim 50\%$ of all intermediatemass, z~0.6 galaxies, since 60% of intermediate-mass, z~0.6 galaxies are indeed starbursts (Hammer et al. 1997; Mignoli et al. 2005). The HST/ACS images and kinematic maps for a representative sub-sample of the IMAGES-CDFS can be found in Fig. 6 (see App. A).

3. ASSOCIATING KINEMATIC DISTURBANCES WITH PHYSICAL PROCESSES

Stellar kinematic disturbances are indubitable evidence for an out-of-equilibrium dynamical state. In high-redshift galaxies, deriving spatially-resolved stellar kinematics remains out of reach, and one has to rely on gas kinematics as a best proxy. This implicitly assumes that gas kinematics traces the gravitational potential, and that no other mechanisms are perturbing gaseous motions, such as, e.g., outflows. In the IMAGES sample, large-scale outflows have been detected in only a handful of cases (Puech et al. 2010). Using FORS2 slit spec-

troscopy, Rodrigues et al. (2012) further estimated that only 8% of intermediate-mass galaxies at $z\sim0.6$ have significant outflows. This suggests that gas kinematics is indeed a reliable tracer of the dynamical state of galaxies, at least on large spatial scales. Several dynamical processes are known to be a source of kinematic disturbances. Some of them are local in space, while others are global. Relative to the equilibrium state of rotation (as expected in the intermediate mass range since more massive galaxies are expected to reach a different equilibrium state supported by dispersion), local disturbances are either due to minor mergers or internal instabilities such as clump formation, while global disturbances can be due to major mergers or cosmological gas accretion (Hopkins et al. 2010).

3.1. Local disturbances

In the IMAGES sample, kinematic perturbations are detected over a ≥ 7 kpc spatial scale, which corresponds to the GIRAFFE-IFU spatial resolution element (i.e., two spaxels). They generally affect the galaxies across a significant fraction of their diameter, which, in principle, excludes de facto any mechanism resulting in local kinematic disturbances. In order to quantify this, we derived the Jeans scale length L_J (Bournaud et al. 2009) in the IMAGES-CDFS, which is found to be 0.7 ± 0.1 kpc. L_I increases to 1.0±0.4 kpc in the sub-sample of clumpy galaxies that show rotation (Puech 2010). Thus, such Jeans instabilities should remain largely undetected at the GIRAFFE IFU spatial resolution. In the bottom of Fig. 2 one of the most clumpiest galaxy in the IMAGES-CDFS sample. This galaxy shows at least seven clumps spread over its disks and is classified as CK. However, the kinematic perturbations are mostly large-scale, with a misalignment between the morphological and kinematic axis as defined by the location of the maximal and minimal rotation velocities, and with a velocity dispersion peak that cannot be reproduced by the rotation model inferred from the VF Yang et al. (2008); Puech et al. (2010). This confirms that even in the most disturbed clumpy galaxies, the kinematic perturbations cannot be associated with the position of the clumps, i.e., they are not local but global. In addition, clump instabilities are limited to a fraction of 20% of intermediate-mass galaxies at $z\sim0.6$ that are effectively clumpy (Puech 2010), which also rules out clump instabilities as a driver for the strongest kinematic perturbations.

Regarding minor mergers, such processes are also expected to lead to local kinematic perturbations only. An obvious case of minor merger with a mass ratio of $\sim 1:18$ was studied in detail by Puech et al. (2007): only a local signature is found in the velocity dispersion map (see top panel in Fig. 2). Even if we cannot exclude that in very specific cases such local processes could result in large kinematic disturbances such as those observed in IMAGES galaxies, we can safely conclude that they cannot be the main driver for the majority of galaxies, at least for the CK galaxies. This does not mean that minor mergers are not ongoing in the IMAGES sample, but given the spatial resolution of GIRAFFE-IFU data, they probably remain mostly undetected.

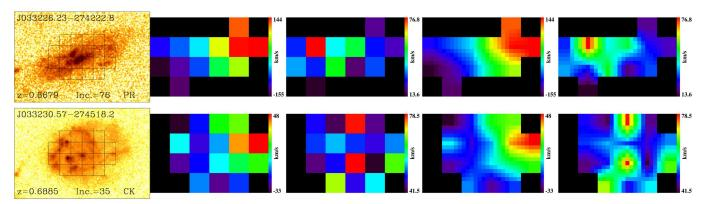


Figure 2. Examples of large-scale kinematic maps obtained in the frame of the IMAGES-CDFS survey with FLAMES/GIRAFFE at VLT. From left to right: HST/ACS z-band image superimposed with the GIRAFFE IFU grid (0.52 arcsec/spaxel), velocity field, velocity dispersion map, 5×5 linearly interpolated velocity field, and 5×5 linearly interpolated velocity dispersion map. Top panel: J033226.23-27422.8, which is an example of a minor merger detected at $z\sim0.67$ (see Puech et al. 2007). Bottom panel: J033230.57-274518.2, which is an example of a $z\sim0.69$ clumpy galaxy with Complex Kinematics. The local perturbations due to minor mergers or local instability remain undetected in the velocity field at the GIRAFFE spatial resolution (see text).

Regarding the impact of processes resulting in global disturbances, it is instructive to consider the range of the relative variations of the gravitational potential (compared to the dynamical equilibrium state) $\Delta \phi / \phi$, in which galaxies can be considered as isolated and subject to secular evolution, as a function of mass and redshift (Hopkins et al. 2010). We estimated $\Delta \phi/\phi$ for galaxies in the IMAGES-CDFS sample using rotation kinematic models (Puech et al. 2008). For this, we derived the pixel-by-pixel relative difference between the observed VF and each galaxy model, and considered the sum $\Delta V/V$ of this map over all pixels, weighted by the observed S/N in each pixel. The quantity $2.\Delta V/V$ can then be used as a proxy for $\Delta \phi/\phi$. We also derived the dynamical timescale t_{dyn} for each galaxy in the IMAGES-CDFS sample using as a proxy the ratio between the gas radius and the rotation velocity as determined by Puech et al. (2010). In galaxies showing rotation (RDs+PRs), we found that $\Delta \phi/\phi = 1.2 \pm 0.4$ (median value) and t_{dyn} =60±3 Myr, while for CK galaxies, $\Delta \phi / \phi = 3.1 \pm 1.0$ and $t_{dyn} = 60 \pm 24$ Myr. Uncertainties correspond to 1- σ error-bar, and were estimated using bootstrap resampling.

In this regime (i.e., $t_{dyn} \gtrsim 10$ Myr and $\Delta \phi / \phi \gtrsim 1$), the two dominant physical processes expected to drive gravitational perturbations in this range of mass and redshifts are secular evolution (i.e., instabilities occurring in a galaxy) and the direct dynamical evolution of individual substructures due to some previously initiated perturbation, which can eventually dominate the evolution of the whole system (Hopkins et al. 2010). Large global perturbations (i.e., $\Delta \phi/\phi \gtrsim 1$) are typically triggered by major mergers. The characteristic timescale for secular evolution can be estimated using the circular disk period i.e., $P_d = 2\pi R/V_c$, with R the disk radius and V_c the circular velocity. We used again gas radius and the rotation velocity as determined by Puech et al. (2010) as proxies for these two quantities. The timescale for dynamical friction associated with the dynamical evolution of substructure was estimated following the simplified prescription given by Hopkins et al. (2010):

$$t_{df} = \frac{0.2}{\delta_0 ln(\Lambda)} P_d,$$

where $\delta_0 = \Delta \phi/\phi$, and $\Lambda = 1+1/\delta_0$. This timescale quantifies how fast the dynamical evolution of substructures evolve on their own, once they have been triggered. For instance, a merging galaxy will trigger instabilities in the main progenitors that will subsequently evolve on their own, on a timescale given by t_{df} (Hopkins et al. 2010). The dominant process at given amplitude of perturbation is the one associated with the shortest timescale.

In Fig. 3, we plotted the expected range of value of these two regimes at $z\sim0.6$ in the IMAGES-CDFS sample. Secular evolution is found to be dominant at small relative variations of the gravitational potential $\Delta \phi / \phi$, while the influence of (major) mergers dominate above $\Delta \phi/\phi \geq 0.3$. More specifically, isolated galaxies should be found in the upper left region of Fig. 3, close to the grey region (as well as large local disks such as M31), while on-going mergers and mergers remnants should be found at $\Delta\phi/\phi \sim 1$ and close to the red region. Comparing with these theoretical expectations, CK galaxies lie closer to the individual dynamical perturbation regime (i.e., the merger-driven regime), which is consistent with (major) merger-driven kinematic disturbances in these galaxies. Galaxies showing rotation also lie in this regime, although with a smaller range of gravitational perturbation, which is consistent with these galaxies being more (temporally) advanced merger remnants, as suggested by their other morpho-kinematic properties (see Hammer et al. 2009 and Sect. 4.1). On overall, z~0.6 rotators (RDs+PRs) lie closer to the expected merger-driven regime, which probably reflects the fact that they are closer to dynamical equilibrium than CK galaxies, in which gravitational perturbations are about three times larger. This suggests that any other known process (gas accretion or secular evolution) is very unlikely to be responsible for the high level of kinematic disturbance observed on large spatial scales, at least for the majority of the IMAGES-CDFS sample.

3.3. Comparison with major merger models

In this context, it was explored whether hydrodynamical major merger models for the 27 galaxies in the IMAGES-CDFS sample which are not relaxed morphogically and/or kinematically could generally account for their perturbations (Hammer et al. 2009,b; Puech et al.

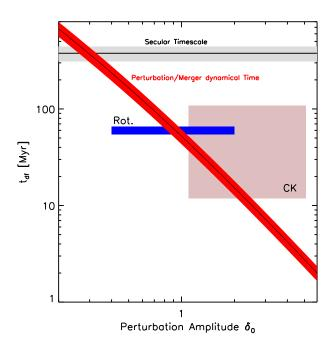


Figure 3. Dynamical timescales (in Myr) for the evolution of secular or self-amplified perturbations as a function of the amplitude of the gravitational perturbation. The grey region represents the expected $2\text{-}\sigma$ uncertainty range around the median timescale for secular perturbations, while the red region represents the expected $2\text{-}\sigma$ uncertainty range around the median timescale for individual perturbations to evolve on its own (as approximated by Eq. (5) of Hopkins et al. 2010, see text). The blue region is the $2\text{-}\sigma$ uncertainty range around the median value obtained for rotating objects at z~0.6, while the brown region represents the same for objects with a complex kinematics.

2009; Peirani et al. 2009; Fuentes-Carrera et al. 2010). Morphological and kinematic maps from these simulations were produced and degraded to the spatial resolution of the observations. Such maps were then explored visually as a function of time and viewing angles to determine the best match to observations. The sodetermined best model was graded by three different examiners (independent of the one who determined the best model) using specific constraints (Hammer et al. 2009). Secure major merger candidates (18/27) were identified as galaxies having a model that fitted observations with a good level of confidence (i.e., grades $\geq 4/6$). Examples of such models are shown in App. A. These candidates can be used as a basis to estimate the fraction of mergers and the merger rate at different epochs as detailed in Sect. 4.1. Interestingly, the modeling exercise lead to a median merger mass ratio μ =3.03±0.34 in the IMAGES-CDFS sample, while theoretical expectations from variations of the gravitational potential give consistent predictions with $\Delta\phi/\phi \sim \mu = 3.1 \pm 1.0$ in CK galaxies (see above). We refer the reader to Hammer et al. (2009) for more details about the comparison between simulations and observations. This comparison suggests that at least 33% of $z\sim0.6$ galaxies (50% of galaxies not relaxed morpho-kinematically according to the morphokinematic classifications × the ratio of secured models, which is 18/27=66%) are involved in major mergers with a median mass ratio ~ 3 .

4. DERIVING THE MERGER RATE OUT TO Z \sim 1.5 FROM MORPHO-KINEMATIC OBSERVATIONS

4.1. Methodology

All the merger phases that are expected to lead to a significant SFR enhancement, i.e., the pre-fusion, fusion/post-fusion, and relaxation phases (Larson & Tinsley 1978), are homogeneously populated as a function of time by the IMAGES-CDFS galaxies, as evidenced by Fig. 4. In this figure, SFRs were homogenized by dividing the observed SFR by the estimated mass of gas in each galaxy and multiplying each derived number by the average mass of gas in the sample. The time sequence reproduces quite well expectations from modeling the star formation during a typical merger (see insert). This shows that morpho-kinematic data such as those provided by the IMAGES survey are sensible to all the phases of a gas-rich major merger event.

Amongst the galaxies populating the relaxation phase, six of them are rotating, but they are clearly distinct of local rotating disks because of their high average star formation rate, and higher gas velocity dispersion (Puech et al. 2007; Epinat et al. 2010). latter suggests that these galaxies are possibly observed during a post major merger relaxation phase (Robertson & Bullock 2008; Monreal-Ibero et al. 2010; see also Fig. 3 and Sect. 3.2). Most of the star formation activity is indeed concentrated at the disk outskirts, which suggests an ongoing inside-out growth of their disks (Neichel et al. 2008; Hammer et al. 2009). The time sequence in Fig. 4 empirically accounts for a cosmological distribution of merger parameters, since it is constructed using a representative sample. It can thus be used to estimate accurately the evolution of the merger fraction and merger rate as follows.

Theory usually gives the merger rate at the time when halos start merging, i.e., where galaxies that inhabit these halos are still in pair. The epoch when a given merging system was still a pair is dated using individual numerical models from Hammer et al. (2009). An homogeneous and self-consistent determination of the merger rate as a function of lookback time can be estimated by simply counting the fraction of galaxies in each phase and dividing this number by the corresponding average visibility timescale provided by the modeling of IM-AGES galaxies. This method assumes that the visibility timescales do not evolve with redshift. Such an assumption is consistent with semi-analytic models, which predict almost no evolution of the merger visibility timescale as a function of lookback time, at least within uncertainties (Kitzbichler & White 2008). Another possible caveat is the observed evolution of the galaxy gas fraction with redshift (Puech et al. 2010; Daddi et al. 2010; Rodrigues et al. 2012; Erb et al. 2006), which could potentially result in evolving timescales depending of the merging phase probed (Lotz et al. 2010b). However, hydrodynamical simulations of binary mergers (Lotz et al. 2010b) predict that unequal mass ratio mergers (which dominate the empirical distribution of merger mass ratios, see Sect. 3.2) generally show no evolution of the pair visibility timescale with gas fraction.

> 4.2. The fraction of mergers out to z~1.5 4.2.1. Pre-fusion and post-fusion phases

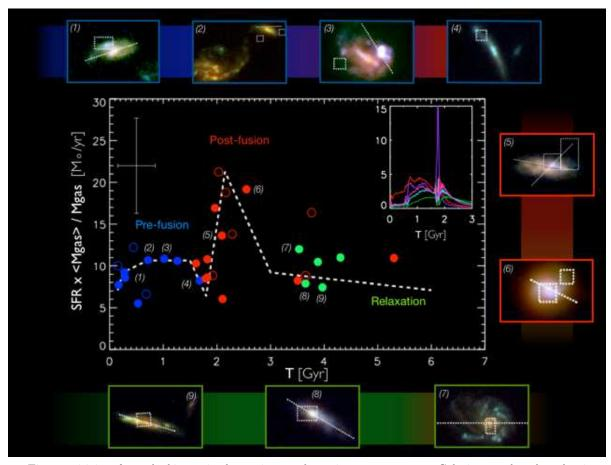


Figure 4. Time sensitivity of morpho-kinematic observations to the major merger process. Galaxies are plotted at the time at which individual numerical models give the best-fit to observations. Full symbols represent galaxies whose morpho-kinematics compared best with those of their models. Merging galaxies were classified into three different classes: the pre-fusion (blue symbols), post-fusion (red), and relaxation phases (green). The pre-fusion phase corresponds to major mergers where both progenitors can be visually identified, while the post-fusion phase corresponds to those where the fusion is too advanced to reliably distinguish them. The dash line is not a fit but a simple visual guide through the points. The median uncertainty is indicated is the upper-left corner. The upper-right inset shows typical similar curves as reproduced from hydrodynamical simulations of major merger (Cox et al. 2006). Surrounding stamps show IMAGES-CDFS HST/ACS B-V-z color images with the approximate location of the kinematic axes (dash white lines) and velocity dispersion peaks (white dash boxes) superimposed. These stamps are numbered in increasing time sequence: (1) J033224.60-274428.1, (2) J033220.48-275143.9, (3) J033239.72-275154.7, (4) J033227.07-274404.7, (5) J033230.43-275304.0, (6) J033245.11-274724.0, (7) J033237.54-274838.9, (8) J033241.88-274853.9, and (9) J033212.39-274353.6. Their morpho-kinematic observations are shown in Fig. 6 as well as the result of their modelling by Hammer et al. (2009), see Appendix A.

Depending on whether or not the two progenitor candidates potentially involved in the merger could be identified visually in the HST/ACS images (e.g., when two candidates for the progenitor nuclei could be identified), the secured major merger candidates were split into prefusion (8 gal.) or post-fusion phases (10 gal.). Amongst the objects that could not be secured as major merger candidates using numerical models, three were found to correspond to the pre-fusion phase, since they reveal distinct potential progenitors. They were therefore added to the pre-fusion phase. We attribute the fact that their numerical models did not succeed in reproducing their morpho-kinematical properties with sufficient precision to the limited exploration of the parameter space.

The pre- and post-fusion phases as observed at $z\sim0.6$ correspond to galaxies that were on average in pairs (and before the first passage) at earlier epochs. To date these epochs, we simply averaged the time elapsed since the beginning of the merger model for each of the 18 secured major merger candidates, and converted these numbers into a redshift. All numbers were weighted by the re-

spective grade given to the different models. It was found that the pre-fusion phase corresponds on average to $z\sim0.72^{+0.10}_{-0.04}$ (i.e., 0.7 ± 0.2 Gyr earlier than z=0.6), while the post-fusion phase corresponds on average to $z\sim1.12^{+0.13}_{-0.10}$ (i.e., 2.5 ± 0.4 Gyr earlier than z=0.6). Uncertainties were estimated using bootstrap resampling.

The fraction of mergers in emission-line galaxies at z=0.4-0.75 for the pre-fusion phase is $0.5 \times 11/33 = 16.7\%$ (with the factor 0.5 accounting for the fact that only one galaxy in the pair is part of the sample), while the fraction of mergers in emission-line galaxies for the post-fusion phase is directly given by 10/33 = 30.3%. Since 60% of intermediate-mass galaxies at $z\sim0.6$ are emission-line galaxies (Hammer et al. 1997; Mignoli et al. 2005), this translates into a total fraction of mergers of 10.0% and 18.1% for the pre- and post-fusion phases, respectively. This assumes that major mergers produce a star formation activity that results in $EW_0([OII]) \geq 15\mathring{A}$. However, it has been shown that major mergers can lead to modest SFR enhancement over relatively short timescales (Di Matteo et al. 2008; Cox et al. 2008;

Robaina et al. 2009; Jogee et al. 2009). This assumption can therefore lead to possible systematic effects that are considered separately (see Sect. 4.4). Random uncertainties due to statistical fluctuations in the respective sub-samples (see Tab. 1) are derived accurately using a beta distribution generator as an estimator of confidence intervals for the binomial statistics (Cameron 2011).

The 18 secured pre- and post-fusion major merger models were used to determine the fusion time for each galaxy. The fusion time was defined as the interval of time between the beginning of the simulation (i.e., when the two progenitors are in pair and before the first passage) and the time at which the two nuclei merge according to the best-fit model. These individual timescales were averaged to mitigate uncertainties due to statistical fluctuations in the respective sub-samples. The averaged pre-fusion phase is found to be 1.8 ± 0.1 Gyr long, which gives an estimate of the pre-fusion visibility timescale in the IMAGES-CDFS sample. The uncertainty was derived by bootstrap resampling of the grade-weighted distribution of individual timescales. We assume the same visibility timescale for the post-fusion phase, since both appear to be similar in the IMAGES sample, according

We compare this estimate with hydrodynamical simulations including radiation transfer (Lotz et al. 2008). We selected the G2 and G3 models as being the closest to the IMAGES-CDFS galaxies in terms of baryonic mass and gas fractions. Indeed, the most important parameters driving the result of a major merger are the baryonic mass (as a proxy for the total mass inside the optical radius) and the gas fraction (Hopkins et al. 2009c). For these two models, the timescale from the beginning of the interaction to the fusion of the two nuclei is found to be 1.24 and 2.44 Gyr respectively, with an average ~ 1.84 Gyr, in good agreement with our estimate² of 1.8 ± 0.1 Gyr. We also compared the pre-fusion visibility timescale with an average pair visibility timescale for large projection distances (i.e., $R_{proj} \leq 100 \text{ kpc.} h^{-1}$) derived from similar simulations (Lotz et al. 2010,b), which is found to be 1.81±0.06 Gyr. Taking into account predictions of mass ratios from galaxy formation models slightly reduces the average value to 1.5-1.6 Gyr (Lotz et al. 2011). The pre-fusion phase includes galaxies that are too close to be selected as pairs by usual criteria (see also Sect. 4.3). It is therefore expected that the pre-fusion visibility timescale in the IMAGES-CDFS sample is slightly larger than the average pair visibility timescale.

4.2.2. Relaxation phase

The six rotating spiral disks in the IMAGES-CDFS can be used to estimate the fraction of mergers at even earlier epochs (see Sect. 3.2 and 4.1). Their mass doubling timescale T_{sfr} is provided by the ratio between their total SFR and stellar mass (Neichel et al. 2008). Note that this timescale is independent of the IMF. One of them shows a very large T_{sfr} (\sim 7 Gyr) and was therefore considered as an interloper and discarded in the following. Assuming that these objects are merger remnants, one can attribute most of their star formation activity to the

formation of the disk (see Sect. 4.1 and 6.2). Therefore, this timescale can be used to roughly estimate the average time elapsed from fusion to the observation epoch of these galaxies. On average, these galaxies were therefore observed as pairs at a lookback time 1.8+1.8 (pre-fusion + post-fusion phases) + 0.5x($< T_{sfr} >$ -1.8) = 3.9±0.3 Gyr, with $< T_{sfr} >$ =2.3±0.3 Gyr (where the error-bar was estimated using bootstrap resampling). This corresponds to z~1.55 $^{+0.15}_{-0.13}$. The average relaxation timescale is found to be 5.5-1.8-1.8=1.9 Gyr (see Fig. 4).

Amongst the nine non- or semi-relaxed galaxies in the IMAGES-CDFS sample that could not be securely identified as major mergers, six were found to be in the postmerger phase according to their best models. They were all modeled quite at the end of the 3 Gyr duration of the simulations, which suggests that the morpho-kinematics of these galaxies might not have been identified as resulting from a major merger due to the limited duration of the simulations. Amongst them, four show evidence for rotation in their velocity fields and were classified as perturbed rotators, which is consistent with this interpretation. We therefore included them as part of the relaxation phase (see red points in the relaxation phase in Fig. 4). This leads to a fraction of mergers at $z\sim1.6$ of 20.0% (see Tab. 1).

4.3. Merger rates

The merger rate r [Gyr⁻¹] corresponding to the three merger phases considered above (i.e., the pre-fusion, post-fusion, and relaxation phases) can be estimated using the ratio between the corresponding merger fraction and visibility timescale (see Tab. 1). Error-bars due to random fluctuations in the sub-samples were estimated by propagating the random uncertainties on the fraction of mergers and on the visibility timescale. The derived merger rates and their associated uncertainties are shown in Fig. 5.

For selection criteria similar to those of the IMAGES-CDFS sample, a fraction of galaxies in pair ~2-6% at $z\sim0.6$ is generally found (Rawat et al. 2008; Kartaltepe et al. 2007; Bundy et al. 2009). present study, the fraction of galaxies involved in major mergers is found to be $10\pm3\%$ at $z\sim0.7$. Such a fraction is larger than the fraction of galaxies in pairs since the pair technique only picks up progenitors when they are approaching for the first time and do not consider progenitors between the first and second passage and/or when they are getting too close one from each other, while morpho-kinematic data are sensitive to all phases. This is reflected in the visibility timescale associated with pair fractions, which is often assumed to be ~ 0.5 Gyr from analytic arguments or independent simulations (i.e., which do not necessarily reflect the exact properties of the observations; see also Lotz et al. 2011). Using such a timescale and a fraction of galaxies in pair $\sim 2-6\%$ indeed leads to a merger rate $\sim 4-12\%$ Gyr^{-1} , which is consistent with our $z\sim0.7$ estimate of 5.5%. When no lower limit to the distance between the two progenitors is imposed, the pair technique gives very similar results, with $\sim 9\%$ of galaxies in pair at $z \sim 0.75$, and $\sim 15\%$ at $z \sim 1$ (Ryan et al. 2008).

The morphological technique provides estimates of the fraction of morphologically-disturbed mergers of 7-11%

² The post-fusion duration was not measured in these simulations but set to an arbitrary time after the coalescence of the nuclei, which prevents any further comparison.

Table 1

Galaxy merger rate derived from the IMAGES-CDFS survey. From left to right: Merger fraction, merger rate, and redshifts sampled by the IMAGES-CDFS survey. Quoted uncertainties correspond to $1-\sigma$ random and systematic error-bars respectively.

Merger phase	Fraction of mergers (%)	Merger rate $(\%.Gyr^{-1})$	Redshift
Pre-fusion	$10.0^{+5.8}_{-2.6}^{+3.3}_{-3.7}$	$5.5^{+3.5}_{-1.8}^{+1.9}_{-2.0}$	$z = 0.72^{+0.10}_{-0.04}$
Post-fusion	$18.1^{+6.7}_{-3.8}^{+3.3}_{-5.5}$	$10.1^{+4.3}_{-2.7}{}^{+1.8}_{-3.3}$	$z = 1.12^{+0.13}_{-0.10}$
Relaxation	$20.0^{+6.8}_{-4.0}^{+3.3}_{-9.1}$	$11.1^{+4.4}_{-2.7}^{+1.8}_{-5.1}$	$z = 1.55^{+0.15}_{-0.13}$

at $z\sim0.7$, 11-17% at $z\sim1.1$, and $27\pm11\%$ at $z\sim1.4$ for similar mass ranges and depending and the method used (CAS/GM system, see Conselice et al. 2008; Lotz et al. 2008; Conselice et al. 2009, or visual inspection, see Bridge et al. 2010; Jogee et al. 2009). Within uncertainties, this is consistent with the fraction of mergers found using morpho-kinematic data (see Tab. 1).

We conclude that alternative techniques generally give consistent estimates, although with a resulting large range of values (Hopkins et al. 2009), which reflects systematic effects due to their limited sensitivity to the merging process and different sample selection effects (see also Lotz et al. 2011).

4.4. Systematic uncertainties

A first possible cause of systematic effects is linked to the selection criteria of the IMAGES-CDFS sample, and in particular to the criterion $EW_0([OII]) \geq 15 \text{Å}$. Indeed, we assumed that all quiescent $(EW_0([OII]) < 15\text{Å})$ galaxies are not major mergers, whereas a significant fraction of them (25%) were found to have peculiar morphologies (Delgado-Serrano et al. 2010), which could be linked to less active mergers. Indeed, numerical simulations have revealed that major mergers do not always lead to strong enhancements of the star formation rate (Di Matteo et al. 2008), and therefore these peculiar quiescent galaxies might also be undergoing major merger events. This could potentially rise the fraction of mergers by 10.0% since quiescent galaxies represent 40% of intermediate-mass galaxies at $z\sim0.6$ (Delgado-Serrano et al. 2010). Since we do not have kinematic data for these objects, this could potentially affect any of the three merger phase considered in this study. We therefore considered that, on average, the merger fraction in each phase could be affected by a $\sim 3.3\%$ systematic effect upward (see Tab. 1).

The number of mergers in the pre-fusion phase could also be overestimated due to fly-by interlopers. We estimated that four out of the eleven objects in this phase could be possible fly-byes and escape a subsequent merger (J033217.62-274257.4, J033219.32-274514.0, J033220.48-275143.9, J033238.60-274631.4). These objects correspond to cases where the two potential progenitors are well separated and photometric redshifts are consistent, but no reliable spectroscopic information was available to confirm whether or not the two galaxies were indeed gravitationally bound. This can potentially have an impact on the fraction of mergers in the pre-fusion phase by 3.7% downward, and the corresponding merger rate by 2.0% (see Tab. 1).

Six galaxies in the IMAGES-CDFS are consistent with expectations from clumpy galaxies (Puech 2010), i.e., gas-rich Toomre-unstable disks. These six galaxies are found to be in the post-fusion phase (3 out of 6). Since

the numerical merger models do not consider small-scale perturbations such as clumps, these galaxies might correspond to Toomre-unstable disks driven by internal instabilities, rather than major mergers. The post-fusion fraction of merger and merger rate might therefore be affected by a 5.5% and 3.3% effect downward, respectively (see Tab. 1). The impact on the pre-fusion and relaxation phases is marginal (one object) compared to other uncertainties, so we did not consider it further.

Regarding the relaxation phase, we added six objects corresponding to the post-fusion phase but which were not safely identified as mergers. This could be due to insufficiently long evolution times, so that the objects could not be safely identified, or to a too limited exploration of the parameter space. Considering these six galaxies as possible interlopers for the relaxation phase, this would impact the corresponding fraction of merger and merger rate by a 9.1% and 5.1% effect downward, respectively (see Tab. 1).

Systematic uncertainties are shown as a grey region in Fig. 5.

5. COMPARISON WITH SEMI-EMPIRICAL MODELS

Instead of trying to predict galaxy properties all the way from initial conditions given by the CMB, semi-empirical models by-pass the unknown coupling between dark and baryonic matter using empirical relations, such as gas fraction or stellar mass functions as a function of redshifts. Such an approach allows us to overcome several issues encountered with semi-analytic models, which can lead to significantly underestimate the merger rate (Hopkins et al. 2010b). The semi-empirical model used here (Hopkins et al. 2009) was shown to reproduce a number a local galaxy properties, such as their bulge-to-disk flux ratio distribution, Tully-Fisher relation, or luminosity function of luminous infrared galaxies (Hopkins et al. 2010c).

5.1. Model parameters

We used the Hopkins et al. (2009) semi-empirical model³ to predict the merger rate in a given range of baryonic mass $[M_b^{min}(z), M_b^{max}(z)]$, gas fraction $[f_{gas}^{min}(z), f_{gas}^{max}(z)]$, and baryonic mass ratio between the two progenitors $[\mu_b^{min}(z), \mu_b^{max}(z)]$ as a function of redshift z. Indeed, Hopkins et al. (2009,c) emphasized that the most appropriate mass would be the tightly bound material that survives stripping to strongly perturb the primary, which is found to be the baryonic plus tightly bound dark matter mass within a few disk scale lengths. The best observable proxy for this quantity is the baryonic mass (Hopkins et al. 2009),

 $^{^3}$ available at https://www.cfa.harvard.edu/ $\sim\!$ phopkins/Site/mergercalc.html as an IDL code.

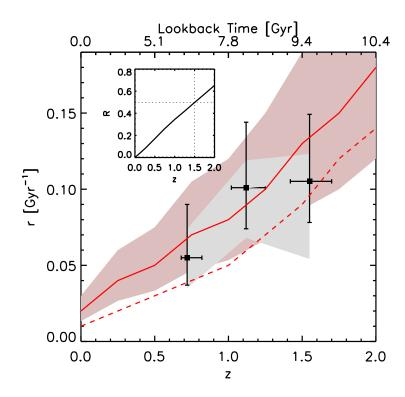


Figure 5. Galaxy merger rate out to z~2. The black points with horizontal and vertical error bars show the observational estimates of the merger rate r from the IMAGES-CDFS sample. The grey-shaded region shows the impact of possible systematic effects of the observational estimation of the merger rate (see Tab. 1). The red curve shows the prediction of the semi-empirical model (Hopkins et al. 2009), for the range of baryonic mass and mass fraction observed. The shaded red region shows the random uncertainty associated to the theoretical prediction (see Sect. 5.2). The dashed-red line shows the impact of systematic uncertainties in stellar mass stellar population models on model predictions (see Sect. 5.2). The upper-left inset shows the cumulative merger rate R as a function of lookback time (i.e., from the full-red curve of the main panel).

which was therefore used in this study. In most studies, the galaxy merger rate is estimated in a fixed range of stellar or baryonic mass, constant with redshift, i.e., $[M_b^{min}(z), M_b^{max}(z)] = [M_b^{min}, M_b^{max}]$. Here, we need to estimate the proper range of baryonic mass $[M_b^{min}(z), M_b^{max}(z)]$ at all z in order to sample the progenitors and descendants of the IMAGES-CDFS galaxies.

Given $[M_b^{min}(z), M_b^{max}(z)]$, we determined the corresponding range of halo mass $[M_h^{min}(z), M_h^{max}(z)]$ using the relationship between baryonic and halo masses $M_b - M_h$ as provided by the Hopkins et al. (2009) halo occupation model (HOD) using the mass function from Perez-Gonzalez et al. (2009). Using alternative mass functions change the merger rate by less than 1\%. We then estimate the average mass of the progenitor halos at z + dz following Neistein et al. (2006, 2008), i.e., $[M_h^{min}(z+dz), M_h^{max}(z+dz)]$, which is then converted back to $[M_b^{min}(z+dz), M_b^{max}(z+dz)]$ using the M_b - M_h relationship. The HOD model is used to estimate the galaxy merger rate at z + dz in the updated range of baryonic mass. This ensures that the derived galaxy merger rate is integrated over the population of the progenitors of all galaxies within $[M_h^{min}(0), M_h^{max}(0)]$ at z = 0 only, and not over all the mass spectrum, which would overestimate the merger rate compared to estimates from observations. In practice, we set $[M_b^{min}(0)/M_{\odot},\ M_b^{max}(0)/M_{\odot}] \simeq [10^{10.4},10^{11.1}]$ in order to sample the range $[M_b^{min}(z=0.6)/M_{\odot},M_b^{max}(z=0.6)]$ $0.6)/M_{\odot}$]=[10^{10.2},10^{11.0}], which corresponds to the baryonic mass range of the IMAGES-CDFS sample (see Sect. 2). We tested that following the mean progenitor mass instead of the average progenitor mass between the upper and lower limit of the mass range does not change the resulting merger rate significantly.

To test the consistency of the adopted HOD model with the IMAGES sample, we checked that, according to the HOD model, the range of baryonic mass sampled at z=0.6 corresponds to a range in $\log (M_{stellar}/M_{\odot})=[10^{10.0},10^{11.0}]$, which also matches the range of observed stellar mass in the IMAGES sample (see Sect. 2.1). At z=0, the HOD model predicts that the z=0.6 progenitors as defined by their range of baryonic mass as above, will end up in a stellar mass range of $\log (M_{stellar}/M_{\odot})=[10^{10.3},10^{11.1}]$, corresponding to the baryonic mass range of $\log (M_b/M_{\odot})=[10^{10.4},10^{11.1}]$ as quoted above. The evolution in stellar mass as predicted by the HOD model is therefore ~ 0.1 -0.3 dex.

The median gas fraction in the progenitors of the IMAGES-CDFS sample were estimated using their observed SFRs (Hammer et al. 2009). We used this to parameterize the expected gas fraction in the IMAGES-CDFS progenitors and descendants, using $f_{gas} = \{15\%, 32\%, 50\%, 75\%, 90\%\}$ at $z = \{0,0.6,0.72,1.12,1.55\}$. Estimates at z = 0 and 0.6 were derived using local HI measurements and inversion of the Schmidt-Kennicutt relation, respectively (Puech et al. 2010; Rodrigues et al. 2012). Estimates at z = 0.72,

1.12, and 1.55 were derived from the estimated median gas fractions in the pre-fusion, post-fusion, and relaxation phase, respectively (Hammer et al. 2009). The HOD model predicts that the progenitors of z~0.6 ongoing mergers in the IMAGES-CDFS sample are galaxies with stellar mass in the range $\log (M_{stellar}/M_{\odot}) \sim$ $[10^{9.2},10^{10.4}]$. Gas fractions of the order of $\sim 90\%$ in such a range of mass at $z\sim1.5$ is consistent with observational estimates of the gas fraction in more z~1.5 massive galaxies (see discussion in Sect. 6.2). We added a ± 1 - σ scatter of 0.15 dex, which appears to represent well the observed scatter at all z (Hopkins et al. 2009,b; Rodrigues et al. 2012). At given z, the range of gas fraction $[f_{gas}^{min}(z), f_{gas}^{max}(z)]$ over which the merger rate was integrated is interpolated from the $f_{gas}(z)$ relationship as defined above, with an added ± 2 - σ scatter. We explored the impact of a larger ± 3 - σ scatter with no qualitative change in the results. Finally, we set $[\mu_b^{min}(z), \mu_b^{max}(z)] = [\mu_b^{min}, \mu_b^{max}] = [0.25, 1.0]$, as found in the IMAGES-CDFS sample (Hammer et al. 2009).

5.2. Comparing observations and theory

Figure 5 compares the derived estimates of the merger rate with state-of-the-art semi-empirical Λ -CDM models (Hopkins et al. 2009). This theoretical model is found to be in remarkable agreement with the observed estimates without any particular fine-tuning. At the redshifts and masses probed by the IMAGES-CDFS sample, semi-empirical (HOD-based) models can predict the merger rate within a factor ~ 1.5 (Hopkins et al. 2010b). HOD models are in relatively good agreement one with each other because they rely on observational constraints (e.g., the galaxy stellar mass function) that are well constrained at z<1 and for stellar masses around M^* (Hopkins et al. 2010b). As stated, above, changing the galaxy stellar mass function changes the resulting merger rate by less than $\sim 1\%$. The dominant source of random uncertainty is therefore due to variations from one (HOD) model to another, which is illustrated in Fig. 5 as a red region. This is the same order of magnitude that random uncertainties associated to the observed merger rate (see Tab. 1). This implies that random uncertainties limit the comparison between observations and theory at a level of a factor ~ 2 .

In this comparison, we adopted a diet Salpeter IMF for all observables at any epoch. Several studies suggest that the IMF might become top-heavy under extreme starburst conditions (Weidner et al. 2010). This could result in an evolution of the IMF with redshift, which would impact the estimation of stellar mass by up to \sim -0.18 dex (rising almost linearly with redshift from z=0 to $z\sim1.5$) compared to estimates at z=0(van Dokkum & van der Marel 2007). This could result in a systematic shift of the merger rate with redshift. Several systematic effects associated with the stellar population models can also affect the determination of the stellar mass. The most significant effect is the influence of the TP-AGB phase, which omission in stellar population models as those used in the present study can lead to overestimate the stellar mass by 0.14 dex (Pozzetti et al. 2007). In addition, using simplified prescriptions for deriving the stellar-mass instead of full SED modelling (Bell et al. 2003), when used at high redshifts, can also potentially lead to overestimate stellar masses by 0.2 dex (Puech et al. 2008; Gallazzi & Bell 2009).

In order to bracket the upper limit of the predicted merger rate at all redshifts, we combined quadratically the systemic uncertainty associated with a possible evolution of the IMF, and the effects of stellar population models, since they are independent. This results in a total systematic uncertainty of -0.27 dex on the baryonic mass. In Fig. 5, we plotted theoretical predictions with $[M_b^{min}(z), M_b^{max}(z)]$ -0.27, using a dashed-red line. In doing so, $[f_{gas}^{min}(z), f_{gas}^{max}(z)]$ was updated accordingly (upward). All these systematic uncertainties associated to the estimation of the stellar mass tend to decrease the galaxy merger rate at all redshifts. However, the theoretical predictions remain consistent with the observational estimates within the corresponding range of observational systematic uncertainties. Quantitatively, this could decrease the integrated merger rate by $\sim 20\%$.

We conclude that the major merger rate is determined from both theory and observations within a factor 2-3, accounting for random and systematic uncertainties. Such an agreement between the merger rate determined using morpho-kinematic data and theoretical predictions without any particular fine-tuning, is remarkable. This is an improvement of a factor ~ 3 compared to previous comparisons between observations and theory (Hopkins et al. 2009).

6. DISCUSSION

6.1. One third of $z\sim0.6$ galaxies are on-going major mergers

Using morpho-kinematic data of z~0.6 galaxies from the IMAGES-CDFS survey, we derived the evolution of the major merger rate out to $z\sim1.5$, i.e., nine billion years ago. Using comparisons of the spatially-resolved morpho-kinematic properties between observations and a grid of hydrodynamical simulations of galaxy mergers, we constrain their time evolution, which allowed us to accurately date back when they were still in pair. In this comparison, the estimate of the merger rate at z~1.5 is much more uncertain since it relies on the relaxation phase during which it is more difficult and/or degenerate to interpret morpho-kinematic features as merger relics. However, it makes sense to interpret such galaxies as post-mergers in the relaxation phase as detailed above, and Fig. 3 & 4 indeed suggest a plausible causal link between distant merging galaxies and such dynamically hot rotating disks. We found a remarkable agreement between these new observational estimates and predictions from state-of-the-art semi-empirical Λ -CDM models within a factor 2-3, accounting for both random and systematic uncertainties.

As a test of consistency, the Λ -CDM model predicts a large fraction of peculiar galaxies at z=[0.4-0.75], which is found to be < r > (i.e., the average merger rate at z=0.65, \sim 0.06 Gyr⁻¹, see Fig. 5) \times τ (i.e., the total duration of the average major merger at z=0.65, \sim 5.5 Gyr, see Fig. 4) \sim 33%. This corresponds exactly to the fraction of observed galaxies in which the peculiar morphologies and/or kinematics can be reproduced by a major merger model (see Sect. 3.2). The Λ -CDM model therefore predicts that \sim 33% of the progenitors of local disks were destroyed over the past 9 Gyr during major

(i.e., baryonic mass ratio $\geq 1:4$) merger events, as observed.

The occurrence of 33% of gas-rich major mergers in $z\sim0.6$ galaxies is also consistent with an increase of the scatter of the Tully-Fisher relation at high redshifts (Flores et al. 2006; Kassin et al. 2007; Puech et al. 2008; Covington et al. 2010; Puech et al. 2010) ⁴, and the observed random walk in the specific angular momentum of $z\sim0.6$ galaxies compared to local galaxies (Puech et al. 2007).

6.2. Disk rebuilding of local bulge-dominated spirals

The agreement found between observations and theoretical predictions (see Fig. 5) evidences that 50% (65%) of local galaxies with stellar mass in the range $10^{10.3}$ - $10^{11.1} \rm M_{\odot}$ (see Sect. 5.1) have undergone a major merger (defined here as baryonic mass ratio ≥ 0.25) since z=1.5 (z=2.0). The Hopkins et al. (2009) model takes into account the specific physics involved in gasrich major mergers, which was shown to reproduce the observed local relation between bulge-to-disk ratio and stellar mass (Hopkins et al. 2009,b). This suggests that the time at which local galaxies have undergone their last major merger could be an important factor in determining how they acquired their internal structure (B/T ratio and angular momentum).

Depending on the gas fraction at fusion time, major mergers are well-known to result in ellipticals (through dry mergers), but also in spirals (through gas-dominated mergers). Indeed, hydrodynamical simulations of isolated merging disk galaxies have shown that with a fraction of gas at the fusion time larger than 50%, a significant disk can reform in the remnant (Springel & Hernquist 2005; Robertson et al. 2006; Hopkins et al. 2009c). Note that the required fraction could be smaller with significant cosmological gas accretion (Brooks et al. 2009), but we will adopt 50% as a conservative limit.

The median gas fraction at z=0.6 is found to be $\sim 30\%$ (Puech et al. 2010; Rodrigues et al. 2012). It is therefore likely that major mergers occurring between z ~ 0.6 and z=0 (which involved 20% of local galaxies according to Fig. 5) were relatively dry, probably resulting in galaxies with significant bulges.

The major mergers sampled by the IMAGES-CDFS sample are those occurring between $z\sim1.5$ and $z\sim0.6$ (see Tab. 1). Fig. 5 shows that 50% of local galaxies were involved in a major merger since z=1.5, of which 30% occurred between z=0.6 and z=1.5. Hammer et al.

(2009) have extrapolated the gas fraction in the progenitors of these mergers, and found gas fractions well in excess of the required value of 50% to reform a disk $(\sim 90\%$, see Sect. 5.1). Several measurements of the gas fraction were attempted at $z\sim1.5$ (Daddi et al. 2010; Weinzirl et al. 2011). Most measurements involve relatively massive galaxies ($\sim M_{stellar} = 10^{10.7} - 10^{11.1} M_{\odot}$) and are limited to their half light radius. However, the HOD model predicts that the progenitors of the on-going $z\sim 0.6$ major mergers at z=1.5 should be in a lower range of stellar mass $\sim 10^{9.2}$ - $10^{10.4} \mathrm{M}_{\odot}$. Rodrigues et al. (2012) homogenized gas estimates from the literature to parameterize the evolution with redshift and stellar mass of the gas fraction within the full gas radius. Extrapolating their gas fraction-stellar mass relation at $z\sim1.5$ in the range of mass $10^{9.2}$ - $10^{10.4} \rm M_{\odot}$, one finds that gas fractions at a level of ~ 80 -100% are probably close to average conditions (see Fig. 7 of Rodrigues et al. 2012). The progenitors of all the $z\sim0.6$ on-going major mergers at z=[0.75-1.5] should therefore be rich enough in gas so that a significant disk reform after fusion, as also evidenced by observations of young dust-enshrouded disks at $z\sim0.6$ (Hammer et al. 2009b; Puech et al. 2009).

We emphasize that we have considered here only the "average" results of major mergers since $z\sim2$ and such statements have to be taken at the lowest order only, since one expects significant scatter in the B/T of a major merger remnant as a function of orbital parameters, gas fraction, and feedback (Hopkins et al. 2008, 2009; Governato et al. 2009). We also emphasize that we considered here only a specific range of mass and that the impact of more modest mergers, i.e., with baryonic mass ratio smaller than 0.25 was not considered.

6.3. Is there a disk survival issue?

Results of semi-analytic models suggest that the likeliest channel for the formation of disk-dominated galaxies is a relatively quiet merger history (e.g., see discussion and references in Weinzirl et al. 2009). Of particular interest are local "bulgeless galaxies" (which we define here as galaxies with $B/T \le 0.2$, as generally considered), which are often thought to have undergone their last major merger above z~2. The relatively large fraction of such galaxies is often considered to be in tension with the fraction of major mergers as inferred from predictions of Λ-CDM models (e.g., Stewart et al. 2008). It was argued in Sect. 6.2 that most descendants of IMAGES-CDFS galaxies should lie within early-type spirals. We now examine whether the fraction of mergers found in Fig. 5 is in tension with the observed fraction of local bulgeless galaxies.

Weinzirl et al. (2009) used Bulge+Bar+Disk decompositions on H-band images and found that two-third of local spirals with $M_{stellar}=10^{10.1}$ - $10^{11.6}M_{\odot}$ are bulgeless. Their determination maximizes the fraction of bulgeless galaxies since they removed the contribution of the bar to the central light and followed the common assumption that bars are pure products of secular evolution and not merging (see discussion in Athanassoula 2008). Since the fraction of spirals amongst local galaxies is $\sim 70\%$ (see App. B), this would translate into a maximal fraction of bulgeless galaxies in the local Universe $\sim 46\%$. As Weinzirl et al. (2009) argued, their sample appears to be representative of the B-band luminosity function

⁴ It has been recently claimed that the distant stellar mass TF relation might have a scatter that is actually similar to the local relation (Miller et al. 2011). The reduced scatter has been attributed to the long integration times that would better sample the plateau of the rotation curve combined to an optimal velocity extraction method, providing a more accurate circular velocity estimation. We note that exposure times in the IMAGES survey are comparable or even larger that those used in this study. Moreover, IFU data provide additional element of resolutions in the direction perpendicular to the galaxy major axis, which provide more information to accurately deconvolve the line-of-sight velocity measurement and estimate the rotation velocity. This is essential when dealing with galaxies with complex VFs, since the kinematic and morphological axes can be significantly misaligned, or when deconvolving the measurement from seeing effects. It is beyond the scope of this paper to provide a definitive assessment on the evolution of the scatter of the TF relation with redshift.

at $M_{stellar} \ge 10^{10.1} M_{\odot}$ (see their Fig. 2). However, their Fig. 3 evidences that their sample can be representative of stellar mass function only above $M_{stellar} \ge 10^{10.6} M_{\odot}$. In this range of mass, the maximal fraction of local bulgeless is found to be 61%, or 43% of local galaxies. Assuming that such galaxies cannot be formed by mergers, this would therefore limit the fraction of major merger in local galaxies since z=2 to 57%. We re-derived Fig. 5 for the range of mass $\rm M_{stellar}{=}10^{10.6}{-}10^{11.6}M_{\odot}.$ Indeed, the HOD model used in the present study predicts that on-going major merger in the z~0.6 IMAGES-CDFS sample should end up in a stellar mass range of 10^{10.3}- $10^{11.1} \rm M_{\odot},$ which is shifted to smaller mass relative to the range $10^{10.6} \text{--} 10^{11.6} \rm M_{\odot}$ in which the Weinzirl et al. (2009) sample is representative. In this higher range of mass, we found that the fraction of local galaxies that have undergone a major merger since z=2 decreases from 65% to 53%. Within uncertainties, this matches quite well the maximal fraction of bulgeless galaxies found by Weinzirl et al. (2009) in the same range of mass (57%).

We conclude that there is no tension between the fraction of mergers inferred from morpho-kinematic data and the fraction of local bulgeless galaxies. In other words, there is no need for disks to survive major mergers in the Λ -CDM paradigm, at least at z<2.

6.4. Disk rebuilding in the cosmological context

The results of this paper point toward a re-building of half of local disks during the past 9.4 Gyr after their last gas-rich major merger (Hopkins et al. 2009,b; Hammer et al. 2005; Stewart et al. 2009). This does not imply that the evolution of the star formation and stellar mass densities are primarily driven by such processes over the same period (Robaina et al. 2009; Hopkins et al. 2010c). These results are consistent with recent developments of the Λ -CDM model at earlier lookback times (i.e., z>1.5), according to which galaxy formation would be mainly driven by streams of cold gas, rather than by major mergers (Förster-Schreiber et al. 2009; Agertz et al. 2009; Weinzirl et al. 2011). Indeed, cosmological simulations predict that cold flows are strongly suppressed below $z\sim1-1.5$ (Keres et al. 2009). Such an epoch might correspond to a transition between two different mechanisms driving galaxy formation, i.e., cold gas streams and gas-rich major mergers, as suggested by the strong evolution of the fraction and properties of clumpy galaxies as a function of redshift (Puech 2010; Contini et al. 2012b). In such simulations, halos with a relatively quiet merger history are usually selected as the best probes for the formation of local thin disks (e.g., Brook et al. 2012). The present results suggest that gasrich major mergers could be be an equally plausible way of forming large thin disks. Further work will be needed to quantify what is the main reservoir of gas from which such thin disks can reform. Potential sources of gas include gas expelled during the merger and which falls back onto the remnant (Barnes 2002), gas coming from external gas accretion (Brooks et al. 2009), and/or gas recycled through stellar feedback (Martig & Bournaud 2010). This emphasizes the need to further explore how such disks can (re-)form in halos with a more recently active merger history (Governato et al. 2009). Interestingly, recent cosmological simulations conducted with state-of-the-art hydrodynamical codes reveal cold gas disks that have larger extent and specific angular momentum compared to disks formed in former SPH cosmologicial simulations (Torrey et al. 2011; Keres et al. 2011). These simulations show that massive halos (i.e., $M_{halo} \geq 10^{11} M_{\odot}$) have significantly larger SFRs at z=0-2, compared to previous simulations (Keres et al. 2011).

7. CONCLUSION

Using morpho-kinematic data of z=[0.4-0.75] galaxies from the IMAGES-CDFS survey, we derived the evolution of the major merger rate out to $z\sim1.5$, i.e., nine billion years ago. Using comparisons of the spatially-resolved morpho-kinematic properties between observations and a grid of hydrodynamical simulations of galaxy mergers, we constrain their time evolution, which allowed us to accurately date back when they were still in pair. We then compared constrains from observations with predictions from semi-empirical models. Our main conclusions are as follows.

- Morpho-kinematic observations are found to be sensitive to all the phase of the merger process, from the pre-fusion phase in which galaxy nuclei are still separable by visual inspection, to the postfusion and relaxation phases, in which the two progenitors merge and progressively reach equilibrium. Each of the three phases are found to last ~1.8 Gyr.
- 2. The major merger rate (defined as baryonic mass ratio ≥ 0.25) inferred from morpho-kinematic observations is found to be evolving from 5.5%.Gyr⁻¹ to 11.1%.Gyr⁻¹ between z=0.72 to z=1.55 in the range of stellar mass 10^{10} - $10^{11}\mathrm{M}_{\odot}$ (diet Salpeter IMF), or $10^{10.2}$ - $10^{11}\mathrm{M}_{\odot}$ in baryonic mass.
- 3. A remarkable agreement is found between observational estimates and predictions from the Hopkins et al. (2009) semi-empirical model, which accounts for the specificity of gas-rich mergers at high redshifts. The agreement is found to be at a level of a factor 2-3 without any particular fine-tuning of the model, accounting for both random and systematic uncertainties on the observational and theoretical sides, which significantly improves the accuracy of previous comparisons.
- 4. The Λ-CDM model predicts, in agreement with observations, that 33% of z~0.6 intermediate-mass galaxies are on-going major mergers. Observational signatures of these mergers encompass morpho-kinematic disturbances in a large fraction of these galaxies at this redshift, and an increase of the scatter of scaling relations between mass, velocity and radius (or angular momentum).
- 5. The $\Lambda\text{-CDM}$ model predicts, in agreement with observations, that 20% / 50% / 65% of local galaxies in the range of stellar mass $10^{10.3}\text{-}10^{11.1}\mathrm{M}_{\odot}$ were involved in a major merger between z=0.6 / 1.5 / z=2.0 and z=0.
- 6. Most of the major mergers occurring between z=0.6 and z=0 were probably relatively dry, resulting in galaxies with a prominent bulge, while most of the major mergers occurring between z=1.5 and

z=0.6 probably involved large gas fractions, which should lead to the rebuilding of a significant disk.

7. Theoretical models often suggest that "bulgeless galaxies" (B/T \leq 0.2) result from relatively quiet merger histories. We found no tension between the fraction of local bulgeless galaxies and the fraction of local galaxies that have undergone a major merger since z=2, i.e., there seems to be no "disk survival issue" but rather a "disk rebuilding" era, at least at z \leq 1.5-2, when the influence of cosmo-

logical gas accretion predicted by theory and simulations would start declining in relatively massive haloes.

This work was partly supported by the "Laboratoire International Associé" Origins. We thank an anonymous referee for her/his careful reading of the paper and thorough comments.

APPENDIX

EXAMPLES OF MORPHO-KINEMATICS DATA AND ASSOCIATED MAJOR MERGER MODELS IN THE IMAGES-CDFS SAMPLE

We present here the i-band HST/ACS images and kinematic maps for a sub-sample of the IMAGES-CDFS, see Fig. 6. Galaxies are the same that those used to illustrate the SFR vs. time sequence of Fig. 4, in the same (i.e., temporal) order, from top to bottom. Galaxies with no major merger model are RDs.

EVOLUTION OF GALAXY MORPHOLOGY BETWEEN $Z\sim0.6$ AND Z=0

We discuss here the evolution of the fraction of morphological types between $z\sim0.6$ and z=0 in the range of stellar mass which encompasses the descendant of the IMAGES-CDFS galaxies.

We estimated the fraction of each morphological type in local galaxies as follows. We first considered Morphologically Determined Luminosity Functions (MDLF) of local galaxies from Nakamura et al. (2003). They indeed constructed LFs for E/S0, S0/a-Sb, Sbc-Sd, and Im galaxies using \sim 1500 galaxies from the SDSS using the r band luminosity. We first converted their observed r band luminosity into stellar mass using prescriptions from Bell et al. (2003), which gives a mean stellar mass/r-band luminosity ratio in the local volume of 3.05 within \pm 30% of systematic uncertainty (diet Salpeter IMF). We then integrated each of the MDLF (once converted into the proper IMF) from $10^{10.3}$ to $10^{11.1} M_{\odot}$, within which the descendants of the on-going $z\sim$ 0.6 major mergers should end up, as predicted by the HOD model (see Sect. 5.1). This results in the fractions of morphological types as listed in Tab. 2. Deriving the fraction of morphological type that way has the advantage of avoiding systematics associated with the representativity of the sample, and is limited only by the statistical scatter associated with the visual classification of Nakamura et al. (2003) and the systematic uncertainty associated to the mean stellar mass-to-light ratio in the local volume as determined by Bell et al. (2003).

As a consistency check, we also derived the fraction of morphological types in the local Universe using the catalogue of ~ 14000 visually classified galaxies in the SDSS from Nair & Abraham (2010). We selected in their catalogue galaxies in the range of mass $10^{10.3}$ - $10^{11.1} \rm M_{\odot}$, and with redshift $z \leq 0.05$. According to their Fig. 1, this select a volume-limited sample in the stellar mass range of interest for our purposes. Nair & Abraham (2010) emphasized that such a cut in z will remove some of the brightest, most massive galaxies in the local volume, but these galaxies are all above the range of mass of interest, so this will not impact the morphological fractions in this range. Derived fractions are also listed in Tab. 2. It is interesting to compare them with those derived by integrating the MDLFs in the local volume, since both derivations rely on completely different selection effects. We also listed results from Delgado-Serrano et al. (2010), which selected a sample of the catalogue from Fukugita et al. (2007), who visually classified a sample of more than 2000 galaxies from the SDSS. Their sub-sample was selected to be volume-limited with $\rm M_{stellar} \geq 10^{10.3} \rm M_{\odot}$ to specifically match the descendants of the galaxies sampled by the IMAGES survey.

The comparison between these three different determinations of the fraction of morphological types in the local Universe in the same mass range reveals interesting features. First, the fraction of spirals is found to be in remarkable agreement, around $\sim 70\%$. There are some variations within the fractions of early-type spirals, probably reflecting the uncertainty associated to eyeball classification between S0 and S0a galaxies. The second interesting feature is the smaller fraction of E/S0 found by Delgado-Serrano et al. (2010) in conjunction with their higher fraction of Peculiar galaxies compared to other catalogues. This was attributed by Delgado-Serrano et al. (2010) to a number a factors that include (1) their systematic use of color maps to identify unusual color gradients, (2) the quantification of the misalignment between bulge and disk centroids, and (3) the compactness of galaxies, which were moved to the peculiar class if too compact to be decomposed into bulge and disk. Galaxies harboring such features were classified as Peculiar by Delgado-Serrano et al. (2010), but are probably in the E/S0 class in other catalogues that do not take into account such an information. This suggests that $\sim 10\%$ of the E/S0 classified by Nakamura et al. (2003) or Nair & Abraham (2010) are actually perturbed and not fully relaxed. Such an interpretation is consistent with the fraction ($\sim 30\%$) of early-type galaxies showing negative color gradients ("blue-cored" early-types) in the local Universe in the SDSS (Suh et al. 2010).

At face value, the fraction of late-type spirals in Tab. 2, i.e., 20-23% might appear in conflict with the fraction of bulgeless spirals derived by Weinzirl et al. (2009), which is found to be $\sim 60\%$ (see Sect. 6.3). We recall that "bulgeless" means here B/T ≤ 0.2 and that the correlation between B/T and morphological type has very large scatter (see, e.g., Fig. 14 of Weinzirl et al. 2009). Selecting galaxies with morphological types in the range Sbc-Sd in the sample of

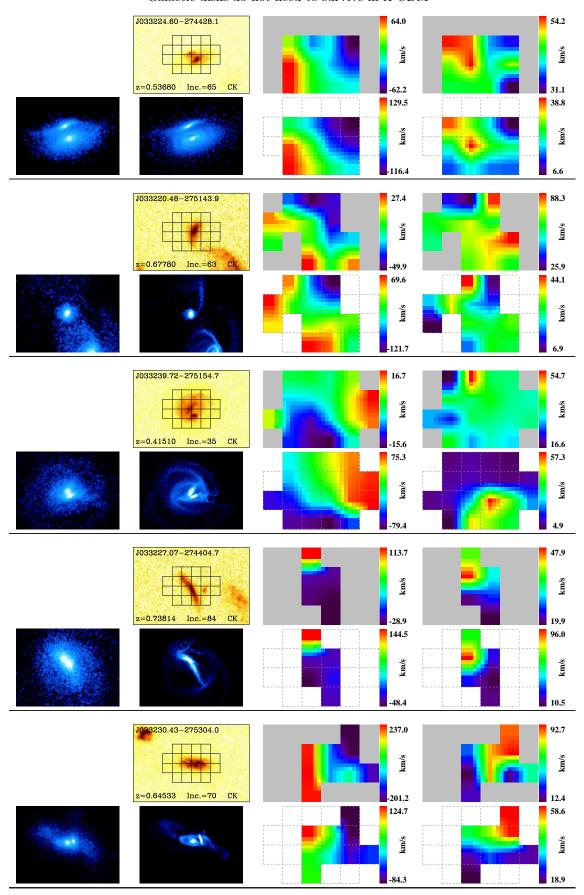
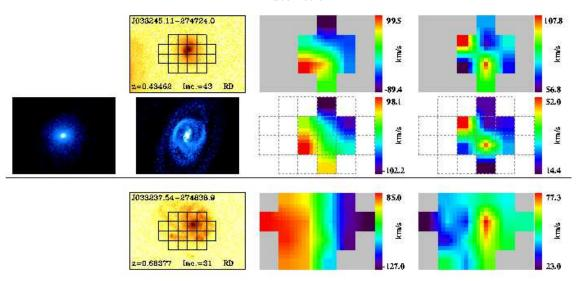


Figure 6. Morpho-kinematic observations for an IMAGES-CDFS subsample and results of their modelling. See text for details. For each galaxy, from left to right: HST/ACS i-band image with the GIRAFFE IFU superimposed, GIRAFFE velocity field, and GIRAFFE velocity dispersion map (top panel), modelled stellar density, modelled gas density, simulated velocity field, and simulated velocity dispersion map (bottom panel). See Hammer et al. (2009) for details.



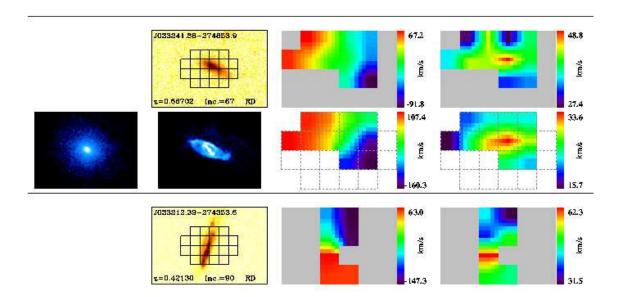


Figure 7. Continued.

Weinzirl et al. (2009) leads to a fraction of late-type galaxies $\sim 33\%$ (above $M_{stellar}=10^{10.6}M_{\odot}$). Since spirals account for $\sim 70\%$ of local galaxies (Tab. 2), this translates into a fraction of $\sim 23\%$ of late-types amongst local galaxies, which is fully consistent with fractions listed in Tab. 2.

We also listed in Tab. 2 the fraction of morphological types found by Delgado-Serrano et al. (2010) at $z\sim0.6$. Note that the fractions of Peculiar galaxies, i.e., those that do not fit into the Hubble sequence, are at both redshifts in very good agreement with those found by van den Bergh (2002). Delgado-Serrano et al. (2010) used exactly the same classification method and strictly equivalent data to classify local and distant galaxies, which minimizes systematics when comparing the two epochs. When one uses the same method, it is found that the fraction of fully relaxed E/S0 does not evolve between $z\sim0.6$ and z=0. Compared to other catalogues, an evolution of the fraction of E/S0 of the order of $\sim10\%$ is found, but this can be attributed to systematics associated to the different classification schemes used. These 10% likely correspond to non-relaxed E/S0, as discussed above.

Table 2

Fractions of morphological type at z=0 in the descendants of the on-going $z\sim0.6$ major mergers. Such remnants are expected in a range of stellar mass $\sim10^{10.3}$ - $10^{11.1} {\rm M}_{\odot}$. The error reflects the uncertainty on the conversion between r-band luminosity and stellar mass (see text). Fractions at z=0 are indicated as derived from Nakamura et al. (2003), Nair & Abraham (2010), and Delgado-Serrano et al. (2010). Note that the sum of the fractions derived from Nakamura et al. (2003) is slightly over 100% because they were derived from the MDLFs. Fractions at z~0.6 were determined by Delgado-Serrano et al. (2010).

Morph. type	Fraction at z=0 from N03	Fraction at z=0 from N10	Fraction at z=0 from DS10	Fraction at z~0.6 from DS10
E/S0	28±3%	31%	18±5%	17±3%
All Sp S0/a-Sd	74+3%	68%	72+8%	31+7%
Early-type Sp	14±3/0	0070	12±0/0	31±1/0
S0/a-Sb	$54\pm4\%$	45%	-	-
Late-type Sp Sbc-Sd	$20{\pm}1\%$	23%		
Im / Pec	20±1% 2+1%	<1%	10+3%	52+9%

REFERENCES

```
Agertz, O., Teyssier, R. & Moore, B. 2009, MNRAS, 397, 64
Arnouts, S. et al. 2007, A&A, 476, 137
Athanassoula, E. 2008, MNRAS, 390, L69
Barnes, J. E. 1988, ApJ, 331, 699
Barnes, J. E. 1992, ApJ, 393, 484
Bell, E.F., McIntosh, D.H., Katz, N. & Weinberg, M.D. 2003, ApJS, 149, 289
Barnes, J. E. 2002, MNRAS, 333, 481
Barnes, J. E., & Hernquist, L. 1996, ApJ, 471, 115
Bell, E.F. et al. 2005, ApJ, 625, 23
Bell E. F., Phleps S., Somerville R. S., Wolf C., Borch A., Meisenheimer K., 2006, ApJ, 652, 270
Bell, E.F. et al. 2007, ApJ, 663, 834
Benson, A. J., & Bower, R. 2011, MNRAS, 410, 2653
Bournaud, F., Daddi, E., Elmegreen, B. G., et al. 2008, A&A, 486, 741
Bournaud, F. & Elmegreen, B.G. 2009, ApJ, 694, 158
Bournaud, F., Elmegreen, B. G., & Martig, M. 2009b, ApJ, 707, L1
Bridge, C.R., Carlberg, R.G. 2010, ApJ, 709, 1067
Brook, C. et al. 2012, MNRAS, 419, 771
Brooks, A. M., Governato, F., Quinn, T., Brook, C. B., & Wadsley, J. 2009, ApJ, 694, 396
Bundy, K. et al. 2009, ApJ, 697, 1369
Cameron, E. 2011, PASA, 28, 128
Ceverino, D., Dekel, A., & Bournaud, F. 2010, MNRAS, 404, 2151
Cirasuolo, M. et al. 2007, MNRAS, 380, 585
Conselice, C.J., Bershady, M.A., Dickinson, M. & Papovich, C. 2003, AJ, 126, 1183
Conselice, C.J., Rajgor, S. & Myers, R. 2008, MNRAS, 386, 909
Conselice, C.J., Yang, C. & Bluck, A.F.L. 2009, MNRAS, 394, 1956
Contini, T., Garilli, B., Le Fvre, O., et al. 2012, A&A, 539, 91
Contini, T., Epinat, B., Vergani, D., et al. 2012b, The Messenger, 147, 32
Covington, M. D., Kassin, S. A., Dutton, A. A., et al. 2010, ApJ, 710, 279
Cox, T.J., Jonsson, P., Primack, J.R. & Somerville, R.S. 2006, MNRAS, 373, 1013
Cox, T. J., Jonsson, P., Somerville, R. S., Primack, J. R., & Dekel, A. 2008, MNRAS, 384, 386
Daddi, E. et al. 2010, ApJ, 713, 686
Dekel, A., Birnboim, Y., Engel, G., et al. 2009, Nature, 457, 451
Dekel, A., Sari, R., & Ceverino, D. 2009b, ApJ, 703, 785
Delgado-Serrano, R. et al. 2010, A&A, 509, A78
de Ravel L., et al., 2009, A&A, 498, 379
de Ravel L., et al., 2011, ArXiv, arXiv:1104.5470
Di Matteo, P. et al. 2008, A&A, 492, 31
Dijkstra, M., & Loeb, A. 2009, MNRAS, 400, 1109
Dutton, A. A., van den Bosch, F. C., & Dekel, A. 2010, MNRAS, 405, 1690 Elmegreen, D. M., Elmegreen, B. G., Rubin, D. S., & Schaffer, M. A. 2005, ApJ, 631, 85
Elmegreen, B. G., Bournaud, F., & Elmegreen, D. M. 2008, ApJ, 688, 67
Elmegreen, B. G., Elmegreen, D. M., Fernandez, M. X., & Lemonias, J. J. 2009, ApJ, 692, 12
Elmegreen, D. M., Elmegreen, B. G., Marcus, M. T., et al. 2009b, ApJ, 701, 306
Epinat B., et al., 2009, A&A, 504, 789
Epinat, B., Amram, P., Balkowski, C., Marcelin, M. 2010, MNRAS, 401, 2113
Epinat, B., Tasca, B., Amram, P., et al. 2012, A&A, 539, 92
Erb, D.K. et al. 2006, ApJ, 646, 107
Faucher-Giguère, C.-A., & Kereš, D. 2011, MNRAS, 412, L118
```

Flores, H., Hammer, F., Puech, M., Amram, P. & Balkowski, C. 2006, A&A, 455, 107 Förster Schreiber, N. M., Genzel, R., Lehnert, M. D., et al. 2006, ApJ, 645, 1062

Förster Schreiber, N. M., Shapley, A. E., Erb, D. K., et al. 2011, ApJ, 731, 65

Frster-Schreiber, N.M. et al. 2009, ApJ, 706, 1364

Robertson, B. et al. 2006, ApJ, 645, 986

Förster Schreiber, N. M., Shapley, A. E., Genzel, R., et al. 2011b, arXiv:1104.0248 Fuentes-Carrera, I. et al. 2010, A&A, 513, A43 Fukugita, M., Nakamura, O., Okamura, S., et al. 2007, AJ, 134, 579 Fumagalli, M., Prochaska, J. X., Kasen, D., et al. 2011, arXiv:1103.2130 Gallazzi A., Bell E. F., 2009, ApJS, 185, 253 Genel S., et al., 2010, ArXiv, arXiv:1011.0433 Genzel, R., Newman, S., Jones, T., et al. 2011, ApJ, 733, 101 Giavalisco, M., Vanzella, E., Salimbeni, S., et al. 2011, arXiv:1106.1205 Goerdt, T., Dekel, A., Sternberg, A., et al. 2010, MNRAS, 407, 613 Governato F., et al., 2009, MNRAS, 398, 312 Hammer, F. et al. 1997, ApJ, 481, 49. u T Hammer, F. et al. 2005, A&A, 430, 115 Hammer, F. et al. 2009, A&A, 507, 1313 Hammer, F. et al. 2009b, A&A, 496, 381 Hernquist L., 1993, ApJ, 409, 548 Hopkins, P. F., Hernquist, L., Cox, T. J., Younger, J. D., & Besla, G. 2008, ApJ, 688, 757 Hopkins, P.F. et al. 2009, ApJ, 715, 202 Hopkins, P.F. et al. 2009b, MNRAS, 397, 802 Hopkins, P.F., Cox, T.J., Younger, J.D. & Hernquist, L. 2009c, ApJ, 691, 1168 Hopkins, P.F., Bundy, K., Hernquist, L., Wuyts, S. & Cox, T.J. 2010, MNRAS, 401, 1131 Hopkins, P.F. et al. 2010b, ApJ, 724, 915 Hopkins, P.F., Younger, J.D., Hayward, C.C., Narayanan, D. & Hernquist, L. 2010c, MNRAS, 402, 1693 Hopkins, P. F., Keres, D., Murray, N., Quataert, E., & Hernquist, L. 2011, arXiv:1111.6591 Jogee, S. et al. 2009, ApJ, 697, 1971 Kartaltepe et al. 2007, ApJS, 172, 320 Kassin, S. A., Weiner, B. J., Faber, S. M., et al. 2007, ApJ, 660, L35 Keres, D., Katz, N., Fardal, M., Dav, R. & Weinberg, D.H. 2009, MNRAS, 395, 160 Keres, D., Vogelsberger, M., Sijacki, D., Springel, V., & Hernquist, L. 2011, arXiv:1109.4638 Kimm, T., Devriendt, J., Slyz, A., et al. 2011, arXiv:1106.0538 Kimm, T., Slyz, A., Devriendt, J., & Pichon, C. 2011b, MNRAS, 413, L51 Kitzbichler, M.G. & White, S.D.M. 2008, MNRAS, 391, 1489 Komatsu, E. et al. 2011, ApJS, 192, 18 Krumholz M. R., Dekel A., 2010, MNRAS, 406, 112 Larson, R.B. & Tinsley, B.M. 1978, ApJ, 219, 46 Law, D. R., Steidel, C. C., Erb, D. K., et al. 2009, ApJ, 697, 2057 Law, D. R., Steidel, C. C., Shapley, A. E., et al. 2012, ApJ, 745, 85 Le Févre, O. et al. 2000, MNRAS, 311, 565 Le Floc'h, E., Papovich, C., Dole, H., et al. 2005, ApJ, 632, 169 Le Tiran, L., Lehnert, M. D., Di Matteo, P., Nesvadba, N. P. H., & van Driel, W. 2011, A&A, 530, L6 Lemoine-Busserolle, M., Bunker, A., Lamareille, F., & Kissler-Patig, M. 2010, MNRAS, 401, 1657 Lemoine-Busserolle, M., & Lamareille, F. 2010, MNRAS, 402, 2291 Lin, L. et al. 2008, ApJ, 681, 232 López-Sanjuan C., Balcells M., Pérez-González P. G., Barro G., García-Dabó C. E., Gallego J., Zamorano J., 2009, A&A, 501, 505 Lotz, J.M., Jonsson, P., Cox, T.J. & Primack, J.R. 2008, MNRAS, 391, 1137 Lotz, J.M. et al. 2008b, ApJ, 672, 177 Lotz, J. M., Jonsson, P., Cox, T. J., & Primack, J. R. 2010, MNRAS, 404, 575 Lotz, J.M., Jonsson, P., Cox, T.J. & Primack, J.R. 2010b, MNRAS, 404, 590Lotz, J. M., Jonsson, P., Cox, T. J., et al. 2011, ApJ, 742, 103 Martig, M., & Bournaud, F. 2010, ApJ, 714, L275 Mignoli, M., Cimatti, A., Zamorani, G., et al. 2005, A&A, 437, 883 Miller, S. H., Bundy, K., Sullivan, M., Ellis, R. S., & Treu, T. 2011, ApJ, 741, 115 Monreal-Ibero, A., et al. 2010, A&A, 517, A28 Murray, N., Quataert, E., & Thompson, T. A. 2010, ApJ, 709, 191 Nair, P. B., & Abraham, R. G. 2010, ApJS, 186, 427 Nakamura, O., Fukugita, M., Yasuda, N., et al. 2003, AJ, 125, 1682 Neichel, B. et al. 2008, A&A, 484, 159 Neistein, E. van den Bosch, F.C. & Dekel, A. 2006, MNRAS, 372, 933 Neistein, E. & Dekel, A. 2008, MNRAS, 383, 615 Noeske, K. G., Weiner, B. J., Faber, S. M., et al. 2007, ApJ, 660, L43 Peirani, S., Hammer, F., Flores, H., Yang, Y.B. & Athanassoula, E. 2009, A&A, 496, 51 Perez-Gonzalez, P.G. et al. 2009, ApJ, 675, 234 Pichon, C., Pogosyan, D., Kimm, T., et al. 2011, MNRAS, 418, 2493 Powell, L. C., Slyz, A., & Devriendt, J. 2011, MNRAS, 414, 3671 Pozzetti, L. et al. 2007, A&A, 474, 443 Puech, M., Hammer, F., Flores, H., Östlin, G., & Marquart, T. 2006, A&A, 455, 119 Puech, M., Hammer, F., Lehnert, M.D. & Flores, H. 2007, A&A, 466, 83 Puech, M. et al. 2007, A&A, 476, 21 Puech, M. et al. 2008, A&A, 484, 173
Puech, M., Hammer, F., Flores, H., Neichel, B. & Yang, Y.B. 2009, A&A, 493, 899 Puech, M. et al. 2010, A&A, 510, A68 Puech, M. 2010, MNRAS, 406, 535 Ravikumar, C.D. et al. 2007, A&A, 465, 1099 Rawat, A., Hammer, F., Kembhavi, A.K. & Flores, H. 2008, ApJ, 681, 1089 Robaina, A. R., Bell, E. F., Skelton, R. E., et al. 2009, ApJ, 704, 324 Robaina A. R., Bell E. F., van der Wel A., Somerville R. S., Skelton R. E., McIntosh D. H., Meisenheimer K., Wolf C., 2010, ApJ, 719, 844 Robertson, B. E., & Bullock, J. S. 2008, ApJ, 685, L27

Rodrigues, M., Puech, M., Hammer, F., Flores, H. & Rothberg, B. 2012, MNRAS, 421, 2888

Ryan R. E., Jr., Cohen S. H., Windhorst R. A., Silk J., 2008, ApJ, 678, 751

Shi Y., Rieke G., Lotz J., Perez-Gonzalez P. G., 2009, ApJ, 697, 1764

Springel, V., & Hernquist, L. 2005, ApJ, 622, L9

Steidel, C. C., Erb, D. K., Shapley, A. E., et al. 2010, ApJ, 717, 289

Stewart, K.R., Bullock, J.S., Wechsler, R.H., Maller, A.H. & Zentner, A.R. 2008, ApJ, 683, 597 Stewart, K.R., Bullock, J.S., Wechsler, R.H. & Maller, A.H. 2009, ApJ, 702, 307

Stewart, K. R., Kaufmann, T., Bullock, J. S., et al. 2011, ApJ, 735, L1

Stewart, K. R., Kaufmann, T., Bullock, J. S., et al. 2011b, ApJ, 738, 39 Suh, H., Jeong, H., Oh, K., et al. 2010, ApJS, 187, 374

Toomre, A., & Toomre, J. 1972, ApJ, 178, 623

Toomre, A. 1977, ARA&A, 15, 437
Torrey, P., Vogelsberger, M., Sijacki, D., Springel, V., & Hernquist, L. 2011, arXiv:1110.5635

Toth, G. & Ostriker, J.P. 1992, ApJ, 389, 5

van den Bergh, S. 2002, PASP, 114, 797

van de Voort, F., Schaye, J., Booth, C. M., Haas, M. R., & Dalla Vecchia, C. 2011, MNRAS, 414, 2458

van Dokkum, P.G. & van der Marel, R.P. 2007, ApJ, 655, 30

van Dokkum, P. G., Brammer, G., Fumagalli, M., et al. 2011, ApJ, 743, 15

van Starkenburg, L., van der Werf, P. P., Franx, M., et al. 2008, A&A, 488, 99

Weidner, C., Kroupa, P. & Bonnell, I.A.D. 2010, MNRAS, 401, 275

Weinzirl, T., Jogee, S., Khochfar, S., Burkert, A., & Kormendy, J. 2009, ApJ, 696, 411 Weinzirl, T., Jogee, S., Conselice, C. J., et al. 2011, ApJ, 743, 87

Wright, S. A., Larkin, J. E., Law, D. R., et al. 2009, ApJ, 699, 421

Yang, Y.B. et al. 2008, A&A, 477, 789

Yang, Y.B., Hammer, F., Flores, H., Puech, M. & Rodrigues, M. 2009, A&A, 501, 437

Zheng, X. Z., Bell, E. F., Papovich, C., et al. 2007, ApJ, 661, L41